An AINTEGUMENTA phospho-switch controls bilateral stem cell activity during secondary growth

Authors: Wei Xiao[1,2,3]†*, Ling Yang[4]†, Hengqi Ji[5], David Molina[1,5], Houming Chen[6], Shan Yu[7], Yingjing Miao[6], Dagmar Ripper[1], Shulin Deng[4], Martin Bayer[1,6], Bert De Rybel[2,3], Laura Ragni[1,5,8]*

Affiliations:

[1]ZMBP-Center for Plant Molecular Biology, University of Tübingen, Auf der Morgenstelle 32, 72076 Tübingen, Germany.

[2]Ghent University, Department of Plant Biotechnology and Bioinformatics, Technologiepark 71, 9052 Ghent, Belgium

[3]VIB Centre for Plant Systems Biology, Technologiepark 71, 9052 Ghent, Belgium.

[4]State Key Laboratory of Plant Diversity and Specialty Crops & Guangdong Provincial Key Laboratory of Applied Botany, South China Botanical Garden, Chinese Academy of Sciences, Guangzhou 510650, China.

[5]Institute of Biology II, University of Freiburg, Schänzlerstr 1, 79104 Freiburg, Germany.

[6]Max Planck Institute for Biology, Department of Cell Biology, Max-Planck-Ring 5, 72076 Tübingen, Germany.

[7]State Key Laboratory of Biocontrol and Guangdong Key Laboratory of Plant Resources, School of Life Sciences, Sun Yat-sen University, Guangzhou, 510275, China.

[8] CIBSS- Centre for Integrative Biological Signalling Studies, University of Freiburg, Germany.

†These authors contribute equally to this work.

*Corresponding author. Email: wei.xiao@psb.ugent.be (W.X.); laura.ragni@biologie.uni-freiburg.de (L.R.)

Key words:

Bilateral stem cell differentiation, Plant secondary growth, ERECTA (ER) pathway, Phosphorylation, AINTEGUMENTA (ANT)

Abstract:

Plant stem cells have the remarkable ability to give rise to distinct tissues and organs throughout development. Two concentric cylinders of actively dividing stem cells are the main drivers of radial thickening during secondary growth, each producing distinct vascular cell types towards the inside and the outside. While the molecular mechanisms underlying their initiation have been well studied, it remains unclear how these stem cell layers determine which cell type is generated. Here, we demonstrate that the cross-talk between the ERECTA (ER) receptor pathway and auxin signalling controls the amount and choice of output tissue in these two stem cell regions. Mechanistically, we show that the ER pathway phosphorylates the transcription factor AINTEGUMENTA, thereby modulating bilateral stem cell activity and favouring the differentiation of only one type of cell. Our results thus show that the phosphorylation status of ANT regulates root girth and biomass accumulation by influencing bilateral stem cell production. This highlights the critical role of post-translational modifications in plant growth and development.

Significance:

This study uncovers a critical regulatory mechanism governing bilateral stem cell activity during plant radial growth. Stem cells in the cambia proliferate and differentiate into specialized tissues like wood and cork, key sites of biomass accumulation. By exploring the interplay between the ERECTA (ER) receptor and auxin signalling, we reveal how these pathways modulate stem cell differentiation and radial thickening through the phosphorylation of the transcription factor AINTEGUMENTA (ANT). Phosphorylation status of ANT modulates stem cell activity, dictating the production of specific vascular cell types like wood thus controlling root girth. This research underscores the importance of post-translational modifications in plant development and provides a novel regulation underpinning stem cell differentiation, with significant implications for enhancing biomass accumulation as wood.

55 **Introduction:**

56 During secondary growth, plant organs undergo a tremendous increase in girth. This is required
57 to provide sufficient mechanical strength during growth and simultaneously increases the
58 capacity of the vascular tissues. In woody plants, most biomass is produced by organs
59 undergoing secondary growth in the form of wood and cork[1,2]. The growth process of
60 secondary growth primarily relies on proliferation within two lateral stem cell zones called the
61 vascular cambium and cork cambium[3-5]. In the Arabidopsis root, these stem cells are organized
62 as two concentric cylinders of dividing cells: the vascular cambium forms the xylem toward
63 the interior and phloem towards the exterior, and all together are referred as the secondary
64 vascular tissues, while the cork cambium produces the periderm with the parenchymatic
65 phelloderm towards the inside and the cork (phellem) towards the outside (**FigS1A**)[6-8]. Despite
66 their structural independence, the relative amount of secondary vascular tissues and periderm
67 produced toward the inside or outside varies in response to plant secondary growth or
68 environmental cues[9,10]. However, the molecular mechanisms that control bilateral output
69 production remain elusive.

70 It is, however, known that phytohormones regulate the self-renewing and differentiation of
71 stem cells in plants[11-13]. For example, recent studies have shown that auxin maxima in
72 proximity to the xylem vessels are required for the initiation and maintenance of vascular
73 cambium activity[14]. Downstream of auxin, AUXIN RESPONSE FACTOR 5/ MONOPTEROS
74 (ARF5/MP) activates the expression of *WUSCHEL-RELATED HOMEOBOX 4* (*WOX4*) and
75 *CLASS III HOMEODOMAIN-LEUCINE ZIPPER* (*HD-ZIPIII*) genes, which regulate cell
76 proliferation[14,15]. During periderm development, auxin accumulates in the cork cambium and
77 controls its initiation by regulating the expression of *WOX4* and *BREVIPEDICELLUS* (*BP*)[7].
78 Furthermore, activation of *BP* and *WOX4* significantly enhances cambial proliferation and
79 leads to an increase in the number of periderm layers[7,15]. Cytokinins (CK) also regulate
80 secondary growth by promoting cell proliferation[16] via transcriptional regulators such as
81 *LATERAL ORGAN BOUNDARIES DOMAIN 3* (*LBD3*), *LBD4*[17], and *AINTEGUMENTA*
82 (*ANT*)[18]. The member of the AP2 transcription factor (TF) family, *ANT,* is first described to
83 control flower organ initiation and maintenance of meristematic competence of plants[19-21].
84 Likewise, it works with cell-cycle player CYCD3;1 to promote cell divisions in the root
85 vascular cambium[18]. Besides phytohormones, several peptides and their respective receptor
86 kinases act as signalling hubs to modulate secondary growth. For example, the leucine-rich
87 receptor-like kinases (LRR-RLK) of the ERECTA (ER) and PHLOEM INTERCALATED
88 WITH XYLEM/TDIF RECEPTOR (PXY/TDR) families control procambium cell

89 divisions[7,14,15,22-30]. Moreover, in hypocotyls, ER recognizes its ligands EPIDERMAL
90 PATTERNING FACTOR (EPF)/EPFL-LIKE (EPFL4/6) and functions in xylem initiation[24].

91 In this study, we show that auxin signalling triggers ER-dependent phosphorylation of ANT.
92 The phosphorylation status of ANT defines whether more cells are generated toward the inside
93 or the outside of the vascular and cork cambium. This ANT-dependent phospho-switch thus
94 serves as a mechanism to precisely control which conductive and protective tissue types are
95 generated by the lateral stem cell niches during secondary growth.
96

97 **Results:**

98 ***Auxin signalling controls the type of secondary tissues produced by lateral stem cell regions***

99 To gain insights into the proliferation dynamics of the vascular and cork cambium stem cell
100 regions involved in secondary growth, we initially performed a quantitative description of these
101 stem cell regions during development (**Fig1A-B** and **S1A-B**). We first focused our attention on
102 the vascular cambium stem cell region by quantifying the number of xylem cells (representing
103 the output toward the inside of the vascular cambium) and the total number of secondary
104 vascular tissue cells (representing the combined bilateral output of the vascular cambium). We
105 sampled the uppermost parts of roots (0.5 cm from hypocotyl) and quantified the
106 aforementioned features before (6-day-old roots), during (8-day-old roots), and after (12-day-
107 old roots) the onset of secondary growth. As an additional control, we included 20-day-old
108 roots with prominent secondary growth (**Fig1A**). The number of secondary vascular cells and
109 secondary xylem cells steadily and significantly increased during secondary growth (**Fig1A-**
110 **B**), which led to a clear expansion of the root girth. The number of secondary xylem cells most
111 prominently increased after day 12, confirming previous results in the hypocotyl region[31].
112 Although a 2-day treatment with the synthetic auxin 1-naphthaleneacetic acid (NAA)
113 significantly increased the total number of secondary vascular tissue cells, there was no
114 significant effect on the number of secondary xylem cells[7,14,15] (**Fig1C-D**). These results
115 indicate that auxin treatment promotes vasculature tissue proliferation but not secondary xylem
116 differentiation.

117 To consolidate these results, we next specifically impaired canonical auxin signalling in the
118 vascular cambium, in an inducible manner using a p*PXY*::*shy2-2*-GR construct[7,32]. Repression
119 of auxin signalling in the vascular cambium suppressed the number of secondary vascular
120 tissues (**Fig1E-F**). To specifically dissect which cell types were affected, we quantified the
121 number of xylem vessels (xylem cells are identified by prominent secondary cell wall
122 accumulation), the number of vascular cambium cells (by expression of the p*PXY*::er-CFP
123 marker), and phloem cells (by subtraction). We observed that impairing auxin signalling in the
124 vascular cambium had a negative effect on the number of phloem and vascular cambium cells
125 in secondary vascular tissues without a significant effect on the number of xylem cells
126 (**FigS1C**). To investigate whether a similar response could be observed in the cork cambium
127 stem cell region, we next quantified the number of cork cells, the total number of periderm
128 cells, and the number of periderm layers[7] during (12-day-old roots) and after (20-day-old roots)
129 periderm formation (**FigS1D-F**). Although the number of periderm layers increased over time,

130 the number of cork layers remained constant, with only a single cork layer (**FigS1D**).
131 Exogenous auxin treatment significantly stimulated cork cambium cell proliferation but
132 exhibited no discernible effect on cork cell formation (**FigS2A-D**). Next, we specifically
133 impaired canonical auxin signalling in the cork cambium in an inducible manner using a
134 p*PER15*::*slr*-GR construct[7,32]. Blocking auxin signalling overall resulted in fewer periderm
135 layers, but an increase in the number of cork cells (**FigS2E-H**). Taken together, these results
136 suggest that auxin is not only required for cell proliferation in the vascular and cork
137 cambium[7,14] but also influences the relative amounts of secondary tissues that are derived from
138 both stem cell regions.

139

140 ***ERECTA controls directional vascular cambium activity downstream of auxin signalling***

141 To uncover how auxin signalling might influence vascular and cork cambium activities on a
142 molecular level, we performed bulk RNA sequencing (RNA-seq) on 12-day-old roots of the
143 p*PXY*::*shy2-2*-GR and p*PER15*::*slr*-GR lines grown on mock or DEX (**FigS3A**). Among the
144 subset of genes significantly repressed by DEX treatment in both lines, we found several known
145 regulators, including *WOX4*, *BP*, *ER, LBD3*, *PIN4* and *ANT* (**FigS3B-C**). These have been
146 demonstrated to promote cork and or vascular cambium activity[7,14,15,18,33] . In Arabidopsis, the
147 ER receptor kinase family comprises three genes: *ER, ER-LIKE1* (*ERL*1) and *ERL2*. They play
148 a role in many aspects of plant development, including maintaining vascular cambium
149 activity[27,29,30]. However, little is known about the underlying mechanism of ER-dependent
150 signalling in this developmental context. As shown for the hypocotyl and stem single*, er, erl1*
151 and *erl2* mutants do not show any vascular phenotypes[24,27,34]. Furthermore, auxin responses
152 were comparable to WT, probably due to compensation mechanisms inside the family
153 (**FigS3D-E**)[24]. To reduce functional redundancy within ER signalling, we next analysed the *er*
154 *erl2* double mutant. Our quantitative analysis revealed that *er erl2* exhibited a trend toward
155 increased xylem vessel number (**Fig2A-B**). Additionally, *er erl2* double mutant did not respond
156 to auxin compared to a WT control (**Fig2A-B**), suggesting a potential connection between the
157 ER pathway and auxin signalling. To further explore the functions of ER signalling during
158 secondary growth, we investigated the effect of ER/ERL signalling inactivation in the cambia.
159 However, the *er erl1 erl2* triple mutant is severely affected in overall growth[29], preventing the
160 analysis of secondary growth and hampering the identification of direct secondary growth
161 phenotypes. To overcome these limitations, we employed tissue-specific expression of an anti-
162 GFP nanobody, which targets the ER-YPet fusion protein for degradation. We introduced this

163 construct in an *er erl1 erl2* triple mutant complemented with a p*ER*::ER-YPet construct[35].
164 Reducing expression levels of ER-YPet in the vascular cambium using this genetic tool led to
165 a reduction in secondary vascular tissues without changing the number of secondary xylem
166 cells (**FigS3F-G**).

167 Given that our transcriptomic data and qPCR results suggested that auxin promotes the
168 expression of *ER* but not *ERL1* and *ERL2* (**FigS3B-C and S4A**), we further focused our study
169 on *ER*. Thus, we examined *ER* expression pattern (p*ER*::NLS-3xVenus) in roots undergoing
170 secondary growth (**FigS4B**)[7]. *ER* expression at the onset of secondary growth was found in the
171 forming vascular cambium and pericycle cells (**FigS4B**), while at later stages in both vascular
172 and cork cambium (**Fig2C**), which resembles the auxin signalling pattern[7,14]. To further dissect
173 a putative role of ER in specifying the output of the vascular cambium, we took advantage of
174 a previously published BAK1-INTERACTING RECEPTOR-LIKE KINASE3 (BIR3)-ER
175 chimera protein[36]. This line allows the activation of the ER pathway in a ligand-independent
176 way. Driving the chimeric BIR3-ER protein from a vascular cambium specific promoter
177 (p*PXY*::BIR3-ER) triggered cell proliferation in the vascular cambium while the number of
178 secondary xylem cells was repressed (**Fig2D-E** and **S4C**). Given that the xylem defects might
179 be due to the fact that *PXY* expression in the vasculature cambium is biased toward the proximal
180 (xylem) side of the cambium and encompasses differentiating xylem, we drove the expression
181 of *BIR3-ER* from a promoter that is expressed in the distal domain of the vascular cambium
182 and in early phloem and overlaps with p*PXY* only in the stem cells of the vascular cambium
183 (*SUPPRESSOR OF MAX2 1-LIKE 5*/*SMXL5*)[37,38]. p*SMXL5*::BIR3-ER roots showed similar
184 phenotypes to p*PXY*::BIR3-ER roots in terms of xylem cell differentiation and secondary
185 vascular tissue formation (**FigS4D).** In addition, in both p*PXY*::BIR3-ER and p*PXY*::BIR3-ER
186 x p*PXY*::er-CFP lines, we observed a broader distribution of dividing vascular cambium cells
187 in secondary vascular tissues as well as ectopic secondary xylem cells (**Fig2F** and **S4E-F**),
188 suggesting that these phenotypes are triggered by the activation of ER signalling in vascular
189 cambium. Collectively, our findings indicate that activation of ER signalling preferentially
190 activates cell proliferation and directs the production of the vascular cambium toward the
191 outside of the root, resulting in more secondary vascular cambium cells.

192

193 ***ER phosphorylates ANT via the MPK6 kinase to determine vascular cambium activity***

194 To explore the potential cross-talk between auxin signalling and ER pathway, we tested
195 whether ER activates well-known auxin-responsive cambial regulators (**FigS3B-C** and

196 **S5A**)[7,15]. *ANT* expression was detected in pericycle, cork cambium and vascular cambium cells
197 (**Fig3A** and **S5B**)[15] and *ANT* levels were specifically increased in p*PXY*::BIR3-ER (**FigS5A**)
198 roots, suggesting that ANT might be activated by the ER pathway.

199 Given that the ER pathway acts by phosphorylating downstream TF targets[39,40], we next
200 explored whether this could occur via the conserved YODA-MKK4/5-MPK3/6 MAPK cascade.
201 This MAP kinase cascade has been shown to function as an integral part of the ER signalling
202 pathway in other developmental contexts, such as embryogenesis and stomatal
203 development[29,30,35,41-44]. Moreover, *MPK6* expression pattern overlaps with *ER* and *ANT* in the
204 cork and vascular cambium (**FigS5C**). Thus, to understand whether MPK6 acts as a
205 downstream component of ER in regulating root secondary growth, we generated lines
206 expressing a dominant negative version of MPK6[45] in the vascular cambium (p*PXY*::MPK6-
207 DN-GFP). Roots harbouring this construct showed a significant increase in the number of
208 secondary xylem cells without impacting overall secondary vascular tissues (**Fig2G-H**). As
209 inactivating the MPK6 pathway resembles *er/erl* deficiency and results in the opposite effect
210 compared to constitutively activating ER (p*PXY*::BIR3-ER) (**Fig2A-B and D-E**), our results
211 suggest that the ER pathway might activate MPK6 to favour directional vascular cambium
212 activity, limiting secondary xylem cells formation.

213 To next explore whether ER might phosphorylate ANT via MPK6, we first conducted an *in*
214 *silico* analysis based on the putative MPK6 target motif to identify potential phosphorylation
215 sites in ANT (**FigS5D**)[46-48]. Four putative phospho-sites were predicted in ANT (S113, S202,
216 T496 and S526) (**FigS5D**). To assess ANT phosphorylation *in vivo*, we then transiently
217 expressed HA-tagged ANT in *Nicotiana benthamiana* leaves in the presence and absence of
218 the Calf-intestinal alkaline phosphatase (CIP) and found that the phosphorylated form of ANT
219 was reduced after CIP treatment (**Fig3B**), indicating that ANT is phosphorylated in *N.*
220 *benthamiana* leaves. Phosphorylation of ANT was increased in the presence of MPK6 and
221 reduced when co-expressed with a dominant negative MPK6 version (**Fig3C**), suggesting that
222 MPK6 can phosphorylate ANT *in planta*. To further support these results, we expressed in *N.*
223 *benthamiana* leaves, a phospho-dead version of ANT, all putative phospho-sites were replaced
224 by alanine (S113A, S202A, T496A and S526A, called ANT-4A) and a phospho-mimic version
225 (ANT-4D) with aspartic acid substitutions at all four sites (S113D, S202D, T496D and S526D).
226 In a Phos-tag gel, we observed only one band for ANT-4A protein corresponding to the non-
227 phosphorylated version, whereas ANT-4D protein mimicked the phosphorylated version
228 (**FigS5D-E**)[49]. Taken together, our data suggest that ER phosphorylates ANT via the MPK6
229 kinase pathway.

230 To next determine if ANT plays a role in modulating vascular cambium activity, we studied
231 the effect of specifically inducing ANT in the vascular cambium (p*PXY*::ANT-GR on DEX).
232 *ANT* induction inhibited vascular cambium differentiation toward the xylem, resulting in fewer
233 secondary xylem cells (**Fig4A-B** and **S6A-B**), highlighting a role for ANT in regulating
234 directional vascular cambium output. Then, we studied the effect of ANT phosphorylation
235 status by comparing the effect of ANT and the ANT-4A expression in the vascular cambium
236 (p*PXY*::ANT-GFP or p*PXY*::ANT-4A-GFP). Constitutive overexpression of *ANT* in the
237 vascular cambium resulted in fewer xylem vessel cells (**FigS6C-D**), while expression of the
238 phospho-dead version resulted in a milder phenotype (**FigS6C-D**), highlighting a role for ANT
239 phosphorylation in regulating directional vascular cambium activity. To further understand the
240 functions of ANT, we generated an inducible chimeric repressor construct by fusing ANT with
241 an EAR-repression domain (SRDX) (p*PXY*::ANT-SRDX-GR)[50]. Induction of *ANT-SRDX*
242 (p*PXY*::ANT-SRDX-GR on DEX) in the vascular cambium triggered a reduction of secondary
243 vascular tissues while xylem cell number was increased (**Fig4C-D** and **S6E-F**), confirming that
244 ANT balances vascular cambium output.

245 To corroborate our hypothesis that ANT is phosphorylated by the ERECTA pathway, we tested
246 whether the effect of ER constitutive activation could be suppressed by reducing ANT function.
247 Induction of p*PXY*::ANT-SRDX-GR in p*PXY*::BIR3-ER lines was able to rescue the xylem
248 deficiency phenotype and secondary vasculature tissue overproduction of p*PXY*::BIR3-ER
249 (**FigS3C** and **S7A**), indicating that ANT is downstream of ER signalling. Additionally, we
250 studied the effect of inducing *ANT*, *ANT* phospho-dead (*ANT-4A*), and ANT phospho-mimic
251 (*ANT-4D*) in a background with reduced ER signalling (p*PXY*::NSlmb-vhhGFP4 in the *er erl1*
252 *erl2* triple mutant complemented with p*ER*::ER-YPet mutants). Only the induction of *ANT-4D*
253 inhibited xylem formation in ER limiting conditions, while the induction of *ANT* and *ANT-4A*
254 did not alter the number of xylem vessels and vascular tissues (**FigS7B-E**), further supporting
255 that ANT phosphorylation is mediated by ER signalling and it is needed for ANT function.
256 Together, these results suggest that ER-MPK6-dependent phosphorylation of ANT controls
257 directional vascular cambium activity and that ANT is an important factor controlling
258 secondary xylem formation.

259

260 ***The ANT-dependent phospho-switch acts in both lateral cambia***

261 Our results showed that both *ANT* and *ER* are expressed in the cork cambium and in the
262 pericycle (the tissue that by divisions, will give rise to the cork cambium) (**Fig2C**, **Fig3A**,

263 **FigS4B**, and **S5D**). Furthermore, the expression was downregulated by blocking auxin
264 signalling in the cork cambium (**FigS3B-C**). Therefore, we hypothesized that a similar ER-
265 ANT-dependent phospho-switch might be active in the periderm to control the directional
266 output of the cork cambium. Indeed, activation of ER specifically in the periderm
267 (p*PER15*::BIR3-ER) increased the number of the periderm cells and layers, while it showed no
268 impact on the number of cork layers (**FigS8A-D**). Reducing expression levels of ER,
269 specifically in the cork cambium using an anti-GFP nanobody approach (p*PER15*::NSlmb-
270 vhhGFP4 in the *er erl1 erl2* triple mutant complemented with p*ER*::ER-YPet) decreased the
271 number of periderm layers and number of periderm cells without affecting the number of cork
272 layers or cork cells (**FigS8E-H**). Moreover, induction of *ANT,* specifically in the cork cambium
273 (p*PER15*::ANT-GR on DEX), resulted in roots with an increased number of periderm layers
274 and cells without alteration of cork layer and cell numbers (**FigS9A-D**). These results thus
275 suggest a similar role for ER in regulating ANT to control directional cork cambium activity.
276 In summary, we proposed that both the vascular and cork cambium share a core regulatory
277 mechanism based on an ER-dependent phospho-switch of ANT to control directional cambium
278 activity (**Fig4E**).

279

280 **Discussion:**

281 Two concentric cylinders of stem cells function in the root to accommodate the vast increase
282 in girth during secondary growth: the vascular and cork cambium (**FigS1A**). Each of these stem
283 cell regions can produce cells towards the inside or the outside, and the relative amounts depend
284 on the phase of development but can be influenced by environmental factors[9,10]. Our results
285 shed light on the molecular regulation of cambium activity by showing that the phosphorylation
286 status of ANT controls this differential output of both cambia (**Fig4E**). ANT is phosphorylated
287 via the ER-MPK6 receptor pathway, and this is promoted by local auxin signalling. As such,
288 this auxin-dependent ANT phospho-switch defines the directionality of the vascular and cork
289 cambium activity and thus controls the relative proportions of cell types being made during
290 secondary growth.

291 What is known to date is that, during plant growth, the ERECTA pathway acts by
292 phosphorylating WRKY TFs during embryogenesis[35,51,52], and *bHLH* TFs during stomata
293 formation[39,43,53-56], and *AP2* factors during radial growth. This suggests that while the ER-
294 MPK6 receptor pathway is conserved, developmental specificity is achieved at the level of the
295 TF family that is phosphorylated. However, *AP2* family TFs such as *BABY BOOM* /

296 *PLETHORA4* (*AP2* family) and *bHLH* family TFs: *TMO5*, *LHW*, and *T5Ls* (*bHLH* family),
297 which are known to regulate cell proliferation during embryogenesis[57] and vascular
298 development[58,59], respectively, is regulated by ER-mediated phosphorylation. An alternative
299 explanation could, therefore, be that only a few ER targets have been identified and that ER-
300 modulated processes share a similar downstream TF module. Future research will show if ER-
301 controlled processes are governed by common core modules of transcriptional regulators of the
302 *AP2*, *bHLH*, and *WRKY* families.

303 Interestingly, a recent study revealed complex regulation of vascular development through the
304 LRR-RLK receptor PXY by its ligand TDIF. Activation of this pathway promotes vascular
305 cambium proliferation via *ANT*/*AIL* (AINTEGUMENTA-like) transcription factors such as
306 *AIL5*/*PLT5* (*PLETHORA 5*), which inhibits xylem vessel and phloem sieve element
307 formation[33]. Furthermore, it has been recently shown that ER forms a complex with PXY,
308 which is needed for PXY-TDIF responses during xylem differentiation[60], raising the question
309 of whether ANT phosphorylation requires ER-PXY complex formation and whether other
310 members of the ANT family are phosphorylated. Interestingly, among the genes downregulated
311 upon blocking auxin signalling in the cambia, we found *AIL5* and *AIL7* (**FigS3C**). Therefore,
312 future research focusing on the interaction of ER with all members of the PXY family (*PXY* is
313 not expressed in the cork cambium[7]) and whether activation of ER/PXY signalling triggers
314 ANT/AILs phosphorylation are necessary to dissect the different contributions and specificity
315 of LRR-RLK receptors in balancing cambia output by ANT/AILs phospho-switch.

316 Altogether, these results place ANT at the cross-talk of several pathways, highlighting the
317 possibility that *ANT* transcript levels and phosphorylation status can be exploited to boost root
318 radial growth and favour the formation of cell types that are relevant for biomass accumulation,
319 such as xylem and cork (**FigS10A-C**). This will be valuable in tree breeding programs aiming
320 to enforce biomass accumulation as wood[61] or in initiatives aiming to store more carbons in
321 the cork and xylem of roots[1,2,62], which represent strategies to mitigate the effects of global
322 warming.

323

324 **Materials and Methods:**

325 <u>Plant material and growth</u>

326 All Arabidopsis mutants and transgenic lines (T1 segregating, F1 crossing, T2 segregating
327 and/or T3 homozygous populations) used in this study are described in **Supplementary Table**
328 **1**. The plants were grown on 1/2MS plates with 1% sugar and 0.8% plant agar. DEX

329 (Dexamethasone) treatment was performed by transferring plants on plates containing 10µM
330 DEX (Sigma, D1756). Auxin treatment was performed by transferring plants to plates
331 containing 1µM NAA (1-naphthaleneacetic acid) plates (1µM, Duchefa, N0903). The
332 Arabidopsis plants were grown *in vitro* under continuous light until sampling, or in soil under
333 long-day conditions (16 hours light versus 8 hours dark) at 22 Celsius degrees.
334
335 Molecular cloning
336 Promoters were amplified from *Arabidopsis thaliana* genomic DNA and protein coding
337 sequence from root cDNA with the primers listed i**n Supplementary Table 2** and cloned into
338 Green Gate entry vectors[63]. All final constructs were assembled with the modular green gate
339 technology[63]. If promoters or protein coding sequences contain BSA I sites, they were replaced
340 as described in[64]. All the modules and vectors used in this study are listed in **Supplementary**
341 **Table 3**. In **Supplementary Table 4**, all the module assembly strategies are described. All
342 final vectors were transformed into *Agrobacterium tumefaciens* GV3101, and *Arabidopsis*
343 *thaliana* plants were transformed via floral dipping. F1 (from crossing) seeds, T1 and T2 seeds
344 selected via fast-red fluorescence seed selection[65] or Homozygous T3 lines were used in this
345 study.
346
347 Histology and fluorescent staining
348 0.5 cm root segments have been collected for plastic embedding (at 0.5 cm below the
349 root/hypocotyl junction). Plastic embedding was performed in Technovit 7100 (Heraeus
350 Kulzer; 64709003) following the manufacturer's instructions and as described in[66]. The plastic
351 sections (5-8 cm) were stained with 0.1 % toluidine blue (Sigma; T3260). The pictures were
352 acquired with a Zeiss Axio M2 imager microscope or a Zeiss Axiophot microscope, with the
353 ZEN Blue software (version 3.4). Suberin was stained by Fluorol yellow (FY), followed the
354 instruction in[67], using Fluorol yellow (Santa Cruz, sc-215052). Propidium Iodide (PI) staining
355 was achieved by directly mounting the root in a 10-30µg/ml solution (Sigma, P4864).
356
357 Confocal Microscopy
358 A Zeiss confocal (LSM880/LSM710) was used to acquire the confocal images with the
359 following settings. For GFP (green fluorescent protein): ex. 488 nm; em. 485–505 nm. For YFP
360 (yellow fluorescent protein), mCitrine and Venus: ex. 514 nm; em. 515–545 nm. For mCherry,
361 RFP, and PI: ex. 561 nm; em. 570–630 nm. For FY: ex. 488nm; em 480-550nm. Orthogonal
362 views of a Z stack were obtained using the ZEN Black software (Zen 2.3 SP1).

363

364 RNA sequencing

365 RNA was extracted from the uppermost 1.5 cm of roots (12-day-old plants) for each sample
366 (Mock or DEX treatment; approximately 100 plants for each sample), using a Universal RNA
367 Purification Kit (Roboklon, E3598-02). RNA quality was checked by Agilent RNA
368 Bioanalyzer chip traces and RNA quantity was estimated using a Nanodrop 2000.
369 The enrichment of mRNA by oligo-dT pull-down was performed using the NEBNext Poly(A)
370 mRNA Magnetic Isolation Module (NEB #E7490L). The construction of RNA libraries was
371 carried out using the NEBNext Ultra II RNA Library Prep Kit for Illumina (NEB #E7530L)
372 with NEBNext Multiplex Oligos for Illumina (Index Primers Set 1 to Set 4). Finally, the RNA
373 library size and quality were measured on DNA High Sensitivity Bioanalyzer chip (Agilent),
374 and RNA libraries were quantified by the NEBNext Library Quant Kit for Illumina (NEB
375 #E7630S).

376 The pair-end 150bp RNA sequencing was performed by Novogene. The analysis of the data
377 was performed using the Galaxy platform (https://usegalaxy.eu/)[68]. Adaptors were removed
378 with Trimmomatic using default parameters, and read quality was assessed with FastQC. Reads
379 were aligned to the TAIR10 genome using Salmon quant using default parameters. Reads were
380 counted using Tximport, and differential gene expression analysis was performed using
381 DESeq2 (**DataS1)**.

382

383 Statistical analyses

384 Quantification, statistical analysis and plotting were performed using in R (version 4.0.3). All
385 box plots were generated using ggplot2 (version 3.4.3). Count data was analysed by fitting
386 generalized linear (mixed) models following poisson (stats package, version 4.0.3), quasi-
387 poisson (stats package, version 4.0.3), or negative binomial (stats package, version 4.0.3).
388 Residual diagnostics of the models were performed using the simulation-based approach of the
389 DHARMa package (version 0.4.6) to select the best fitting model. Inference from the models
390 was done with the emmeans package (version 1.5.5-1) and p-values for the pairwise contrasts
391 were adjusted using the Holm-Bonferroni method. Compact letter display of pairwise
392 comparisons was generated using the multcomp package (version 1.4-16), using a significance
393 level of 0.05. All data and tests used for statistical analyses are summarised in Table S2.

394

395 Cell number quantification, root area, and image analyses

396 The identification of periderm and secondary vascular tissues was based on a group of
397 specialized cells named phloem pools (red asterisks), which demarcated the boundary between
398 these tissue systems, serving as persistent histological markers before, at, and after the
399 secondary growth **(FigS1A-B)[6,7].** The quantification of periderm layers was described in[7]. The
400 cell number quantification was performed by Fiji (https://fiji.sc/)[69]. For every genotype, 8-25
401 cross-sections from independent plants were analysed. 2-3 independent experiments were
402 performed and only one experiment was presented. The cork/xylem/periderm/vasculature
403 tissue cell number was calculated using the cell counter plugin in Fiji. To identify specific cell
404 types within secondary vascular tissues, the p*PXY*::er-CFP marker was introduced into several
405 transgenic lines and this fluorescent marker served as a reliable indicator for distinguishing
406 different cell populations. In vibratome cross-sections, the quantification of xylem cell number
407 is based on secondary cell wall accumulation, the quantification of vascular cambium cells by
408 expression of the p*PXY*::er-CFP marker, and the quantification of phloem cells is calculated by
409 subtraction (the number of secondary growth tissues cells minus the number of xylem and
410 vascular cambium cells). The tissue cell numbers were calculated using the cell counter plugin
411 in Fiji. The area (in pixels) of the root was calculated in Fiji.
412
413 Western blot and phosphorylation assay in *Nicotiana benthamiana* leaves
414 Using the GreenGate cloning system, all CDS were driven by 35S promoter and tagged with
415 HA-tag or FLAG-tag at the C-terminus (details in Table S4). All plant binary vectors were
416 transformed into *Agrobacterium tumefaciens* (strain GV3101). These vectors were cultured
417 overnight and resuspended in the tobacco infiltration buffer [10 mM MES (pH 5.7) and 10 mM
418 $MgCl_2$] for each construct. The selected constructs were co-infiltered with the P19 silencing
419 vector into the leaves of *N. benthamiana* and the infiltrated leaves were collected after 72h.
420 The leaves samples were ground to fine powders in liquid nitrogen, and total proteins were
421 extracted in SDS-loading buffer [62.5 mM Tris-HCl pH 6.8, 2.5 % SDS, 0.002 % Bromophenol
422 Blue, 0.7135 M (5%) DTT, 10 % glycerol, and 12.5 mM Protease Inhibitor Cocktail] followed
423 by heating at 95 °C for 5 min. Calf-intestinal alkaline phosphatase (CIP) (NEB #M0525V) was
424 added to protein samples and incubated at 37°C for 1h. Protein samples were resolved in a
425 Phos-tag (AAL-107, Wako Pure Chemical Corporation) 10% SDS-PAGE gel and analysed by
426 Western blot.
427 The primary antibody Anti-c-HA (Abcam, ab18181, 1:2,500 dilution) and Anti-FLAG
428 Nanobody-HRP (AlpalifebioK, TSM1318, 1:5,000 dilution) and secondary antibody
429 GOAT ANTI MOUSE (Bio-rad, STAR137, 1:20,000 dilution) were selected for the

430 immunoblotting. Signal detection was performed with the Clarity Western ECL Substrate (Bio-
431 rad, 170-5060) and detected by ChemiDoc XRS+ System.
432
433 Vibratome sections for confocal imaging
434 The uppermost 1 cm of roots were collected and fixed in 4% paraformaldehyde (PFA) in Ca^{2+},
435 Mg^{2+}-free PBS. The samples were vacuum infiltrated at RT for 1h. After washing with PBS,
436 samples were embedded in warm 5% agarose (Sigma-Aldrich, A4018). Once the agarose
437 solidified, the blocks were sectioned using a vibratome (Leica, VT1000 S) at a thickness of 80-
438 100 µm per section. The sections were washed 3 times with PBS and stained with 1µg/ml
439 Calcofluor White (Merck, 18909) or 0.05% Direct Red 23 (Sigma, 212490).
440
441 Edu staining
442 The plants were grown on 1/2 MS plates for 17d. Next, plants were collected together with
443 some agar, and transferred into liquid 10µM EdU (Sigma, BCK-EDU488) 1/2 MS medium for
444 16h. The samples were then fixed and sectioned as described in vibratome confocal section
445 above. The cross-sections were collected and submerged by Edu detection cocktail under RT
446 for 1h following manufacturer instructions. The cross-sections were washed 2 times with PBS
447 and stained with 1µg/ml Calcofluor White.

Acknowledgments:

We thank Ari Pekka Mähönen and Peter Etchells for sharing seeds and materials. We thank Andrea Boch and Xudong Zhang for technical help. We thank Perrine Dalby for the initial experiment on the mutants of *ER*. We thank Shihao Su for critical reading of the manuscript. We thank Max Minne and Nataliia Konstantinova for their help with statistical analysis.

Funding:

Research is supported by the German Science Foundation (Deutsche Forschungsgemeinschaft, DFG - grant RA-2590/1-3, SFB1101/B10 to L.R., BA3356/3-1, BA3356/4-1, and SFB1101/B12 to M.B.), the Science and Technology Project in Guangzhou (E33309001-4 to S.D.), and DFG Major Research Instrumentation grants (INST 37/965-1 FUGG and INST 37/819-1 FUGG to the LSM880 and the Arabidopsis walk-in chamber used in this study were acquired).

Author contributions:

W.X, and L.R, conceived the project. W.X, L.Y, M.B and L.R, designed the experiments. W.X, and L.Y, conducted the experiments, and analysed the data. W.X. performed RNA-seq, and W.X, and L.R, analysed the obtained data. W.X, L.Y, H.C, D.M, and Y.M, generated the plant transgenic lines. W.X, H.J. and L.R, acquired the confocal images. W.X, performed the qRT-PCRs and plant embedding. W.X, L.Y, and H.J, cross the plants. W.X, L.Y, and S.Y, performed the phosphorylation experiments. W.X, and L.Y, performed the western blot. W.X, analysed data measurement. W.X., B.D.R. and LR wrote the paper with input from all authors.

Competing interests:

Authors declare that they have no competing interests.

Data and materials availability:

Raw RNA-seq data can be accessed at NCBI with GEO number GSE270329.

Supplementary Materials:

Figs S1 to S10

Tables S1 to S5

Data S1 to S2

Supplementary references (1-14)

483 **Figure Legends:**

484

485 **Fig. 1. Auxin signalling preferential controls the specific output of vascular cambium. (A)**,
486 Secondary growth progression in the Arabidopsis root. Cross-sections of the most mature part
487 of 6-day, 8-day, 12-day, and 20-day roots (*in vitro*). In the left panels, the orange squares
488 indicate the magnification area shown in the right panels. Xylem cells are highlighted in blue.
489 **(B)**, Quantification of secondary vascular (SV) tissue and xylem cell numbers of the
490 experiment shown in (Fig1A). **(C)**, Cross-sections (plastic embedding) of the uppermost part
491 of Col0 roots. 12-day-old plants were transferred to either Mock (left panel) or 1µM NAA
492 (right panel) plates for 2 days. **(D)**, Quantification of the number of secondary vascular tissues
493 and xylem cells in (Fig1C). **(E)**, Cross-sections (plastic embedding) quantification of the
494 uppermost part of p*PXY*::*shy2-2*-GR roots (p*MYB84*::NLS-3xGFP and W131Y background);
495 12-day-old plants were transferred to either Mock (left panel) or 10 µM DEX (right panel)
496 plates for 2 days. **(F)**, Quantification of the number of secondary vascular tissues and xylem
497 cells in (Fig1E). The xylem vessels are highlighted in blue. Black scale bars: 20µm. Count data
498 was modelled with a generalized mixed model. Here the Poisson mix model or Poisson model
499 was selected. P-values were adjusted using Holm-Bonferroni correction.

500

501 **Fig. 2. The ERECTA and MPK6 kinase trigger the directional vascular cambium activity.**
502 **(A)**, Cross-sections (plastic embedding) of the uppermost part of Col0 and *er erl2* roots. 6-day-
503 old plants were transferred for 2 days on Mock (left panels) or 1µM NAA (right panels) plates.
504 **(B)**, Quantification of the number of secondary vascular (SV) tissues and xylem cells in
505 (Fig2A). **(C)**, Vibratome-sections of the uppermost part of 18-day-old p*ER::*3xVenus-N7 root.
506 The red arrow indicates the cork cambium and the green arrow indicates the vascular cambium.
507 **(D)**, Cross-sections (plastic embedding) of the uppermost part of 20-day-old Col0 (left panel)
508 and p*PXY*::BIR3-ER (right panel) roots. The xylem vessels are highlighted in blue. **(E)**,
509 Quantification of the number of secondary vascular tissues and xylem cells in (Fig2D). **(F)**,
510 Edu staining of vibratome-sections of the uppermost part of 20-day-old Col0 (left panel) and
511 p*PXY*::BIR3-ER (right panel) roots. **(G)**, Cross-sections (plastic embedding) of the uppermost
512 part of 20-day-old Col0 (up-left panel) and p*PXY*::MPK6-DN-GFP (up-right panel) roots. The
513 xylem vessels are highlighted in blue. **(H)**, Quantification of the number of secondary vascular
514 tissues and xylem cells in (Fig2G). Black and white scale bars: 20µm. Count data was modelled
515 with a generalized mixed model. Here the Poisson mix model was selected. P values were

516 adjusted using Holm-Bonferroni correction. Count data was also analysed using the Student's
517 T-test.
518
519 **Fig. 3. ER phosphorylates ANT via the MPK6 kinase. (A)**, Vibratome-sections of the
520 uppermost part of 18-day-old p*ANT*::RFP roots. The red arrow indicates the cork cambium and
521 the green arrow indicates the vascular cambium. **(B)**, *In vivo* phosphorylation assays in *N.*
522 *benthamiana.* Protein extracts, with or without treatment with Calf-intestinal alkaline (CIP),
523 were analysed on a Phos-tag SDS-PAGE gel and probed with an anti-HA antibody. **(C)**, *In vivo*
524 phosphorylation assays in *N. benthamiana.* p*35S*::ANT-3xHA were transiently expressed in
525 leaves together with either p*35S*::MPK6-GFP or p*35S*::MPK6-DN-GFP (its dominant negative
526 version). Protein extracts were analysed on a Phos-tag SDS-PAGE gel and probed with an anti-
527 HA antibody. The relative concentration of phosphorylated ANT protein and unphosphorylated
528 ANT protein was calculated using Fiji. White scale bars: 20µm.
529
530 **Fig. 4. ANT determines vascular cambium activity by repressing xylem cell formation.**
531 **(A)**, Cross-sections (plastic embedding) of the uppermost part of 12-day-old p*PXY*::ANT-GR
532 roots; 7-day-old plants were transferred to either Mock (left panel) or 10 µM DEX (right panel)
533 plates for 5 days. **(B)**, Quantification of the number of secondary vascular (SV) tissues and
534 xylem cells shown in (Fig4A). **(C)**, Cross-sections (plastic embedding) of the uppermost part
535 of 12-d-old p*PXY*::ANT-SRDX-GR roots; 7-day-old plants were transferred to either Mock
536 (left panel) or 10 µM DEX (right panel) plates for 5 days. **(D)**, Quantification of the number of
537 secondary vascular tissues and xylem cells shown in (Fig4C). **(E)**, Model explaining cambia
538 output specificity. White scale bars: 20µm. Count data was modelled with a generalized mixed
539 model. Here the Poisson mix model was selected. P values were adjusted using Holm-
540 Bonferroni correction. Count data was also analysed using the Student's T-test.
541
542 **Supplementary Figure Legends:**
543
544 **Fig. S1. Vascular cambium and cork cambium dynamics during secondary growth.**
545 **Related to Figure 1.**
546 **(A)**, Sketches highlighting the different tissues occurring during secondary growth. In the
547 Middle panel, secondary vascular (SV) tissues are highlighted in orange, and the periderm in
548 pink. Left panels: tissues comprising the secondary vasculature tissues: xylem (pale blue),
549 vascular cambium (brown) and phloem (violet). Right panels: tissues comprising the periderm:

550 cork (military green), cork cambium (green) and phelloderm (turquoise). **(B)**, Cross-sections
551 highlighting how the different tissues were morphologically identified and scored. The blue
552 line shows the boundary between the secondary vascular tissues and the periderm. Yellow
553 asterisks indicate pericycle cells and red asterisks indicate the phloem poles. **(C)**, Left panels:
554 vibratome-sections of the uppermost part of p*PXY*::*shy2-2*-GR x p*PXY*::er-CFP F1 plants. 12-
555 day-old plants were transferred to either Mock (left-up panel) or 10 µM DEX (left-down panel)
556 plates for 2 days. Right panel: quantification of the number of xylem cells, vascular cambium
557 cells and phloem cells in left panels. White asterisk indicates xylem cells. **(D)**, Left panels:
558 cross-sections of the most mature part of 12-day-old and 20-day-old roots with highlighted the
559 periderm development. The orange squares indicate the magnification area shown in the middle
560 panels (middle panels). Black dots represent periderm cell layers. Right panels: cross-sections
561 (plastic embedding) stained with Fluorol yellow (FY) of the uppermost part of 12-day-old and
562 20-day-old roots. Yellow dots represent suberized periderm layers and grey dots represent non-
563 suberized periderm layers. **(E)**, Quantification of periderm layers number of the experiment
564 shown in (FigS1D). **(F)**, Quantification of the number of periderm and cork cells in (FigS1D).
565 Black and white scale bars: 20µm. Count data was modelled with a generalized mixed model.
566 Here the Poisson mix model was selected. P values were adjusted using Holm-Bonferroni
567 correction.
568
569 **Fig. S2. Auxin balances the formation of the cork cambium derivatives. Related to Figure**
570 **1.**
571 **(A)**, Cross-sections (plastic embedding) of the uppermost part of Col0 roots. 12-day-old plants
572 were transferred for 2 days on Mock (left panel) or 1µM NAA (right panel) plates. Black dots
573 represent periderm cell layers. **(B)**, Cross-sections of the upper most part of Col0 roots stained
574 with Fluorol yellow (FY). 12-day-old plants were transferred for 2 days on Mock (left panel)
575 or 1µM NAA (right panel) plates. Yellow dots represent suberized periderm layers and grey
576 dots represent non-suberized periderm layers. **(C)**, Quantification of periderm layers of the
577 experiment shown in (Fig S2A). **(D)**, Quantification of the number of periderm and cork in
578 (FigS2A). **(E)**, Cross-sections (plastic embedding) quantification of the uppermost part of 20-
579 day-old p*PER15*::*slr*-GR (p*MYB84*::NLS-3xGFP and W131Y background) roots; 12-day-old
580 plants were transferred for 8 days on Mock (left panel) or 10µM DEX (right panel) plates. **(F)**,
581 Cross-sections of the uppermost part of p*PER15*::*slr*-GR roots with Fluorol yellow (FY). 12-
582 day-old plants were transferred for 8 days on Mock (left panel) or 10µM DEX (right panel)
583 plates. Yellow dots represent suberized periderm layers and grey dots represent non-suberized

584 periderm layers. **(G)**, Quantification of periderm layers of the experiment shown in (FigS2E).
585 **(H)**, Quantification of the number of periderm and cork cells in (FigS2E). Black and white
586 scale bars: 20μm. Count data was modelled with a generalized mixed model. Here the Poisson
587 mix model was selected. P values were adjusted using Holm-Bonferroni correction.
588
589 **Fig. S3. ER is induced by auxin and promotes secondary growth. Related to Figure 2 and**
590 **data S1.**
591 **(A)**, The sketch of the RNA-seq experimental design. 12-day-old plants were transferred for
592 24h on Mock or 10μM DEX plates, and the uppermost 1.5 cm- 2cm was collected for each
593 sample. **(B)**, Venn diagrams show the overlap of genes co-upregulated or genes co-
594 downregulated in p*PER15*::*slr*-GR and p*PXY*::*shy2-2*-GR in Mock or 10μM DEX treatment
595 (log2FC≥0.5 or log2FC≤-0.5; and padj≤0.05). **(C)**, The heatmap of genes regulated by DEX
596 treatment in both p*PER15*::*slr*-GR and p*PXY*::*shy2-2*-GR. **(D)**, Cross-sections (plastic
597 embedding) of the uppermost part of Col0, *erl1*, *erl2* and *er* roots. 6-day-old plants were
598 transferred for 2 days on Mock (left panels) or 1μM NAA (right panels) plates. **(E)**,
599 Quantification of the number of secondary vascular (SV) tissues and xylem cells in (FigS3D).
600 M indicates Mock and N indicates NAA. **(F)**, Cross-sections (plastic embedding) of the
601 uppermost part of 12-day-old p*ER*::ER-YPet, *er erl1 erl2* (left panel), and p*PXY*::NSImb-
602 vhhGFP4 in p*ER*::ER-YPet*, er erl1 erl2* (right panel) roots. The xylem vessels are highlighted
603 in blue. **(G)**, Quantification of the number of secondary vascular tissues and xylem cells in
604 (FigS3F). Black scale bars: 20μm. Count data was modelled with a generalized mixed model.
605 Here the Poisson mix model was selected. P values were adjusted using Holm-Bonferroni
606 correction.
607
608 **Fig. S4. ER controls vascular cambium derivative formation. Related to Figure 2.**
609 **(A)**, Relative expression of *ER*, *ERL1* and *ERL2* in the Col0. 12-day-old plants were transferred
610 for 1 days on Mock or 1μM NAA plates. **(B)**, Orthogonal view of z stacks of p*ER*::3xVenus-
611 N7. 12-day-old roots at the positions corresponding to stage 1 (lower panel, before the initiation
612 of periderm), stages 3 (middle panel, on the initiation of periderm), and stage 5 (up panel, after
613 the initiation of periderm) of secondary growth. The red arrow indicates cork
614 cambium/pericycle and the green arrow indicates vascular cambium**.** PI: Propidium Iodide. **(C)**,
615 Cross-sections (plastic embedding) of the uppermost part of 20-day-old p*PXY*::BIR3-ER (right
616 panel) roots. The blue arrow indicates the ectopic secondary xylem cells. The xylem vessels
617 are highlighted in blue. **(D)**, Upper panels: cross-sections (plastic embedding) of the uppermost

618 part of 13-day-old Col0 and p*SMXL5*::BIR3-ER. Lower panel: quantification of the number of
619 secondary vascular (SV) tissues and xylem cells in (FigS4D). **(E),** Vibratome-sections of the
620 uppermost part of 20-day-old Col0 x p*PXY*::er-CFP (up-panel), and p*PXY*::BIR3-ER x
621 p*PXY*::er-CFP (low-panel) F1 roots. White Asterisk indicates xylem cells. **(F),** Quantification
622 of the number of xylem cells, vascular cambium cells and Phloem cells in (FigS4E)**.** Black and
623 white scale bars: 20μm. Count data was modelled with a generalized mixed model. Here the
624 Poisson mix model was selected. P values were adjusted using Holm-Bonferroni correction.
625
626 **Fig. S5. ANT is phosphorylated by MPK6. Related to Figure 2 and Figure3.**
627 **(A)**, Relative expression of *BP*, *WOX4*, and *ANT* in the Col0 and p*PXY*::BIR3-ER roots. 14-
628 day-old roots for collection. **(B)**, Orthogonal view of Z-stacks of p*ANT*::H2B-YFP. 12-day-old
629 roots at the positions corresponding to stage 1 (lower panel), stages 3 (middle panel), and stage
630 5 (up panel) of secondary growth. The red arrow indicates the cork cambium/pericycle and the
631 green arrow indicates the vascular cambium**. (C),** Upper panels: orthogonal view of Z-stacks
632 of p*MPK6*::NLS-3xmVenus. 14-day-old roots at the positions corresponding to stage 1 (lower
633 panel), stages 3 (middle panel), and stage 5 (up panel) of secondary growth. Lower panels:
634 vibratome-sections of the uppermost part of 15-day-old p*MPK6*::NLS-3xmVenus. The red
635 arrow indicates the cork cambium / pericycle and the green arrow indicates the vascular
636 cambium. PI: Propidium Iodide; DR: Direct Red. **(D)**, Putative MPK6 phosphorylation sites in
637 the ANT sequence. ANT contains two AP2 domains. Four putative MPK6 phosphorylation
638 residues (S113, S202, T496 and S526) were highlighted in the ANT protein. **(E)**, *In vivo*
639 phosphorylation assays in *N. benthamiana.* The p*35S*::ANT-4D-3xFLAG (Phosphor-mimic
640 version of ANT), the p*35S*::ANT-4A-3xFLAG (Phospho-dead version of ANT) and the
641 p*35S*::ANT-3xFLAG vectors were transiently expressed in leaves. Protein extracts were
642 analysed on a Phos-tag/Normal SDS-PAGE gel and probed with an anti-Flag antibody. Black
643 scale bars: 20μm. Count data was modelled with a generalized mixed model. Here the Poisson
644 mix model or Poisson model was selected. P values were adjusted using Holm-Bonferroni
645 correction.
646
647 **Fig. S6. ANT acts downstream ER signalling to control vascular cambium output.**
648 **Related to Figure 3.**
649 **(A),** Vibratome-sections of the uppermost part of p*PXY*::ANT-GR x p*PXY*::er-CFP F1 plants.
650 7-day-old plants were transferred to either Mock (left panel) or 10 μM DEX (right panel) plates
651 for 5 days. White asterisk indicates xylem cells. **(B),** Quantification of the number of xylem

652 cells, vascular cambium cells and phloem cells in (FigS6A). **(C),** Cross-sections (plastic
653 embedding) of the uppermost part of 14-day-old Col0, and T1 of p*PXY*::ANT-GFP and
654 p*PXY*::ANT-4A-GFP roots. The xylem vessels are highlighted in blue. **(D),** Quantification of
655 xylem cell number and secondary vascular (SV) tissues cell number in 14-day-old root shown
656 in (FigS6C). **(E),** Vibratome-sections of the uppermost part of p*PXY*::ANT-SRDX-GR x
657 p*PXY*::er-CFP F1 plants. 7-day-old plants were transferred to either Mock (left panel) or 10 µM
658 DEX (right panel) plates for 5 days. White asterisk indicates xylem cells. **(F),** Quantification
659 of the number of xylem cells, vascular cambium cells and phloem cells in (FigS6E). Black and
660 white scale bars: 20µm. Count data was modelled with a generalized mixed model. Here the
661 Poisson mix model or Poisson model was selected. P values were adjusted using Holm-
662 Bonferroni correction. Count data was also analysed using the Student's T-test.
663
664 **Fig. S7. ANT phosphorylation depends on ER signalling. Related to Figure 3.**
665 **(A),** Upper panels: root cross-sections of p*PXY*::BIR3-ER x p*PXY*::ANT-SRDX-GR. 12-day-
666 old plants were transferred to either Mock (left panel) or 10 µM DEX (right panel) plates for 8
667 days. Lower panel: quantification of 20-day-old root in xylem cell number and secondary
668 vascular tissues cell number of the experiment shown in (FigS7A). **(B-D),** The root cross-
669 sections of T1 p*PXY*::ANT-GR (B), p*PXY*::ANT-4A-GR (C), and p*PXY*::ANT-4D-GR (D) in
670 p*PXY*::NSImb-vhhGFP4 in p*ER*::ER-YPet*, er erl1 erl2* plants. 12-day-old plants were grown
671 on Mock (left panel) or 10µM DEX (right panel) plates. The xylem vessels are highlighted in
672 blue. **(E),** Quantification of 12-day-old root in xylem cell number and secondary vascular
673 tissues cell number of the experiment shown in (FigS7B-D). Black scale bars: 20µm. Count
674 data was modelled with a generalized mixed model. Here the Poisson mix model or Poisson
675 model was selected. P values were adjusted using Holm-Bonferroni correction.
676
677 **Fig. S8. ER balances cork cambium produces. Related to Figure 4.**
678 **(A)**, Cross-sections of the uppermost part of 12-day-old Col0 (left panel) and p*PER15*::BIR3-
679 ER (right panel) roots. Black dots represent periderm cell layers. **(B)**, Cross-sections (plastic
680 embedding) stained with Fluorol yellow (FY) of the uppermost part of 12-day-old Col0 (left
681 panel) and p*PER15*::BIR3-ER (right panel) roots. Yellow dots represent suberized periderm
682 layers and grey dots represent non-suberized periderm layers. **(C)**, Quantification of periderm
683 layers number of the experiment shown in (Fig S8A). **(D)**, Quantification of the number of
684 periderm and cork cells in (FigS8A). **(E)**, Cross-sections of the uppermost part of 12-day-old
685 p*ER*::ER-YPet, *er erl1 erl2* (left panel), p*PER15*::NSImb-vhhGFP4 in p*ER*::ER-YPet*, er erl1*

686 *erl2* (right panel) roots. Black dots represent periderm cell layers. **(F)**, Cross-sections (plastic
687 embedding) stained with Fluorol yellow (FY) of the uppermost part of 12-day-old Col0 (left
688 panel) and p*PER15*::BIR3-ER (right panel) roots. Yellow dots represent suberized periderm
689 layers and grey dots represent non-suberized periderm layers. **(G)**, Quantification of periderm
690 layers of the experiment shown in (Fig S8E). **(H)**, Quantification of the number of periderm
691 and cork cells in (FigS8E). White scale bars: 20μm. Count data was modelled with a
692 generalized mixed model. Here the Poisson mix model or Poisson model was selected. P values
693 were adjusted using Holm-Bonferroni correction.
694
695 **Fig. S9. ANT balances cork cambium derivative formation. Related to Figure 4.**
696 **(A)**, Cross-sections of the uppermost part of 12-day-old p*PER15*::ANT-GR roots; 7-day-old
697 plants were transferred for 5 days on Mock (left panel) or 10μM DEX (right panel) plates.
698 Black dots represent periderm cell layers. **(B)**, Cross-sections (plastic embedding) stained with
699 Fluorol yellow (FY) of the uppermost part of 12-day-old p*PER15*::ANT-GR roots. 7-day-old
700 plants were transferred for 5 days on Mock (left panel) or 10μM DEX (right panel) plates.
701 Yellow dots represent suberized periderm layers and grey dots represent non-suberized
702 periderm layers. **(C)**, Quantification of periderm layers of the experiment shown in (FigS9A).
703 **(D)**, Quantification of the number of periderm and cork in (FigS9A). White scale bars: 20μm.
704 Count data was modelled with a generalized mixed model. Here the Poisson mix model was
705 selected. P values were adjusted using Holm-Bonferroni correction.
706
707 **Fig. S10. Extra secondary xylem cells enhance the plant growth. Related to Figure 4.**
708 **(A)**, Root cross-section of p*PXY*::ANT-SRDX-GR plants grown in Mock/DEX plates for 20
709 day are shown. 12-day-old plants on Mock (up panel) or DEX (lower panel) plates and were
710 transferred to Mock plates. **(B-C)**, Quantification of fresh weight of the shoot **(B)** and area of
711 the root **(C)** is measured in the experiment shown in (FigS10A). White scale bars: 20μm. Count
712 data was modelled with a generalized mixed model. Here the Poisson mix model was selected.
713 P values were adjusted using Holm-Bonferroni correction.
714

715 **References:**

716 1 Pan, Y. *et al.* A large and persistent carbon sink in the world's forests. *Science* **333**,
717 988-993, doi:10.1126/science.1201609 (2011).
718 2 Richardson, A. D. *et al.* Climate change, phenology, and phenological control of
719 vegetation feedbacks to the climate system. *Agric. For. Meteorol* **169**, 156-173,
720 doi:10.1016/j.agrformet.2012.09.012 (2013).
721 3 Barra-Jimenez, A. & Ragni, L. Secondary development in the stem: when
722 Arabidopsis and trees are closer than it seems. *Curr Opin Plant Biol* **35**, 145-151,
723 doi:10.1016/j.pbi.2016.12.002 (2017).
724 4 Campilho, A., Nieminen, K. & Ragni, L. The development of the periderm: the final
725 frontier between a plant and its environment. *Curr Opin Plant Biol* **53**, 10-14,
726 doi:10.1016/j.pbi.2019.08.008 (2020).
727 5 Ragni, L. & Greb, T. Secondary growth as a determinant of plant shape and form.
728 *Semin Cell Dev Biol* **79**, 58-67, doi:10.1016/j.semcdb.2017.08.050 (2018).
729 6 Wunderling, A. *et al.* A molecular framework to study periderm formation in
730 Arabidopsis. *New Phytol* **219**, 216-229, doi:10.1111/nph.15128 (2018).
731 7 Xiao, W. *et al.* Pluripotent Pericycle Cells Trigger Different Growth Outputs by
732 Integrating Developmental Cues into Distinct Regulatory Modules. *Curr Biol* **30**,
733 4384-4398 e4385, doi:10.1016/j.cub.2020.08.053 (2020).
734 8 Serra, O., Mahonen, A. P., Hetherington, A. J. & Ragni, L. The Making of Plant
735 Armor: The Periderm. *Annu Rev Plant Biol* **73**, 405-432, doi:10.1146/annurev-
736 arplant-102720-031405 (2022).
737 9 Agusti, J. & Greb, T. Going with the wind--adaptive dynamics of plant secondary
738 meristems. *Mech Dev* **130**, 34-44, doi:10.1016/j.mod.2012.05.011 (2013).
739 10 Rowe, N. & Speck, T. Plant growth forms: an ecological and evolutionary
740 perspective. *New Phytol* **166**, 61-72, doi:10.1111/j.1469-8137.2004.01309.x (2005).
741 11 Kende, H. & Zeevaart, J. The Five "Classical" Plant Hormones. *Plant Cell* **9**, 1197-
742 1210, doi:10.1105/tpc.9.7.1197 (1997).
743 12 Gray, W. M. Hormonal regulation of plant growth and development. *PLoS Biol* **2**,
744 E311, doi:10.1371/journal.pbio.0020311 (2004).
745 13 Hodge, A. Root decisions. *Plant Cell Environ* **32**, 628-640, doi:10.1111/j.1365-
746 3040.2008.01891.x (2009).
747 14 Smetana, O. *et al.* High levels of auxin signalling define the stem-cell organizer of the
748 vascular cambium. *Nature* **565**, 485-489, doi:10.1038/s41586-018-0837-0 (2019).
749 15 Zhang, J. *et al.* Transcriptional regulatory framework for vascular cambium
750 development in Arabidopsis roots. *Nat Plants* **5**, 1033-1042, doi:10.1038/s41477-019-
751 0522-9 (2019).
752 16 Mahonen, A. P. *et al.* Cytokinin signaling and its inhibitor AHP6 regulate cell fate
753 during vascular development. *Science* **311**, 94-98, doi:10.1126/science.1118875
754 (2006).
755 17 Ye, L. *et al.* Cytokinins initiate secondary growth in the Arabidopsis root through a
756 set of LBD genes. *Curr Biol* **31**, 3365-3373 e3367, doi:10.1016/j.cub.2021.05.036
757 (2021).
758 18 Randall, R. S. *et al.* AINTEGUMENTA and the D-type cyclin CYCD3;1 regulate root
759 secondary growth and respond to cytokinins. *Biol Open* **4**, 1229-1236,
760 doi:10.1242/bio.013128 (2015).
761 19 Elliott, R. C. *et al.* AINTEGUMENTA, an APETALA2-like gene of Arabidopsis with
762 pleiotropic roles in ovule development and floral organ growth. *Plant Cell* **8**, 155-168,
763 doi:10.1105/tpc.8.2.155 (1996).
764 20 Klucher, K. M., Chow, H., Reiser, L. & Fischer, R. L. The AINTEGUMENTA gene
765 of Arabidopsis required for ovule and female gametophyte development is related to

766 the floral homeotic gene APETALA2. *Plant Cell* **8**, 137-153, doi:10.1105/tpc.8.2.137
767 (1996).
768 21 Mizukami, Y. & Fischer, R. L. Plant organ size control: AINTEGUMENTA regulates
769 growth and cell numbers during organogenesis. *Proc Natl Acad Sci U S A* **97**, 942-
770 947, doi:10.1073/pnas.97.2.942 (2000).
771 22 Etchells, J. P., Provost, C. M., Mishra, L. & Turner, S. R. WOX4 and WOX14 act
772 downstream of the PXY receptor kinase to regulate plant vascular proliferation
773 independently of any role in vascular organisation. *Development* **140**, 2224-2234,
774 doi:10.1242/dev.091314 (2013).
775 23 Uchida, N. & Tasaka, M. Regulation of plant vascular stem cells by endodermis-
776 derived EPFL-family peptide hormones and phloem-expressed ERECTA-family
777 receptor kinases. *J Exp Bot* **64**, 5335-5343, doi:10.1093/jxb/ert196 (2013).
778 24 Wang, N. *et al.* Organ-specific genetic interactions between paralogues of the PXY
779 and ER receptor kinases enforce radial patterning in Arabidopsis vascular tissue.
780 *Development* **146**, doi:10.1242/dev.177105 (2019).
781 25 Hirakawa, Y., Kondo, Y. & Fukuda, H. TDIF peptide signaling regulates vascular
782 stem cell proliferation via the WOX4 homeobox gene in Arabidopsis. *Plant Cell* **22**,
783 2618-2629, doi:10.1105/tpc.110.076083 (2010).
784 26 Etchells, J. P. & Turner, S. R. The PXY-CLE41 receptor ligand pair defines a
785 multifunctional pathway that controls the rate and orientation of vascular cell division.
786 *Development* **137**, 767-774, doi:10.1242/dev.044941 (2010).
787 27 Ikematsu, S., Tasaka, M., Torii, K. U. & Uchida, N. ERECTA-family receptor kinase
788 genes redundantly prevent premature progression of secondary growth in the
789 Arabidopsis hypocotyl. *New Phytol* **213**, 1697-1709, doi:10.1111/nph.14335 (2017).
790 28 Uchida, N. *et al.* Regulation of inflorescence architecture by intertissue layer ligand-
791 receptor communication between endodermis and phloem. *Proc Natl Acad Sci U S A*
792 **109**, 6337-6342, doi:10.1073/pnas.1117537109 (2012).
793 29 Shpak, E. D., Berthiaume, C. T., Hill, E. J. & Torii, K. U. Synergistic interaction of
794 three ERECTA-family receptor-like kinases controls Arabidopsis organ growth and
795 flower development by promoting cell proliferation. *Development* **131**, 1491-1501,
796 doi:10.1242/dev.01028 (2004).
797 30 Torii, K. U. *et al.* The Arabidopsis ERECTA gene encodes a putative receptor protein
798 kinase with extracellular leucine-rich repeats. *Plant Cell* **8**, 735-746,
799 doi:10.1105/tpc.8.4.735 (1996).
800 31 Sankar, M., Nieminen, K., Ragni, L., Xenarios, I. & Hardtke, C. S. Automated
801 quantitative histology reveals vascular morphodynamics during Arabidopsis
802 hypocotyl secondary growth. *Elife* **3**, e01567, doi:10.7554/eLife.01567 (2014).
803 32 Vermeer, J. E. *et al.* A spatial accommodation by neighboring cells is required for
804 organ initiation in Arabidopsis. *Science* **343**, 178-183, doi:10.1126/science.1245871
805 (2014).
806 33 Eswaran, G. *et al.* Identification of cambium stem cell factors and their positioning
807 mechanism. *Science* **386**, 646-653, doi:10.1126/science.adj8752 (2024).
808 34 Ben-Targem, M., Ripper, D., Bayer, M. & Ragni, L. Auxin and gibberellin signaling
809 cross-talk promotes hypocotyl xylem expansion and cambium homeostasis. *J Exp Bot*
810 **72**, 3647-3660, doi:10.1093/jxb/erab089 (2021).
811 35 Wang, K. *et al.* Independent parental contributions initiate zygote polarization in
812 Arabidopsis thaliana. *Curr Biol* **31**, 4810-4816 e4815, doi:10.1016/j.cub.2021.08.033
813 (2021).
814 36 Hohmann, U. *et al.* Constitutive Activation of Leucine-Rich Repeat Receptor Kinase
815 Signaling Pathways by BAK1-INTERACTING RECEPTOR-LIKE KINASE3
816 Chimera. *Plant Cell* **32**, 3311-3323, doi:10.1105/tpc.20.00138 (2020).

817 37 Shi, D., Lebovka, I., Lopez-Salmeron, V., Sanchez, P. & Greb, T. Bifacial cambium
818 stem cells generate xylem and phloem during radial plant growth. *Development* **146**,
819 doi:10.1242/dev.171355 (2019).
820 38 Wallner, E. S. *et al.* Strigolactone- and Karrikin-Independent SMXL Proteins Are
821 Central Regulators of Phloem Formation. *Curr Biol* **27**, 1241-1247,
822 doi:10.1016/j.cub.2017.03.014 (2017).
823 39 Pillitteri, L. J., Sloan, D. B., Bogenschutz, N. L. & Torii, K. U. Termination of
824 asymmetric cell division and differentiation of stomata. *Nature* **445**, 501-505,
825 doi:10.1038/nature05467 (2007).
826 40 Liu, T., Ohashi-Ito, K. & Bergmann, D. C. Orthologs of Arabidopsis thaliana stomatal
827 bHLH genes and regulation of stomatal development in grasses. *Development* **136**,
828 2265-2276, doi:10.1242/dev.032938 (2009).
829 41 Bergmann, D. C., Lukowitz, W. & Somerville, C. R. Stomatal development and
830 pattern controlled by a MAPKK kinase. *Science* **304**, 1494-1497,
831 doi:10.1126/science.1096014 (2004).
832 42 Lukowitz, W., Roeder, A., Parmenter, D. & Somerville, C. A MAPKK kinase gene
833 regulates extra-embryonic cell fate in Arabidopsis. *Cell* **116**, 109-119,
834 doi:10.1016/s0092-8674(03)01067-5 (2004).
835 43 Meng, X. *et al.* A MAPK cascade downstream of ERECTA receptor-like protein
836 kinase regulates Arabidopsis inflorescence architecture by promoting localized cell
837 proliferation. *Plant Cell* **24**, 4948-4960, doi:10.1105/tpc.112.104695 (2012).
838 44 Shpak, E. D., McAbee, J. M., Pillitteri, L. J. & Torii, K. U. Stomatal patterning and
839 differentiation by synergistic interactions of receptor kinases. *Science* **309**, 290-293,
840 doi:10.1126/science.1109710 (2005).
841 45 Bush, S. M. & Krysan, P. J. Mutational evidence that the Arabidopsis MAP kinase
842 MPK6 is involved in anther, inflorescence, and embryo development. *J Exp Bot* **58**,
843 2181-2191, doi:10.1093/jxb/erm092 (2007).
844 46 Zhang, M. & Zhang, S. Mitogen-activated protein kinase cascades in plant signaling.
845 *J Integr Plant Biol* **64**, 301-341, doi:10.1111/jipb.13215 (2022).
846 47 Li, H. *et al.* MPK3- and MPK6-Mediated ICE1 Phosphorylation Negatively Regulates
847 ICE1 Stability and Freezing Tolerance in Arabidopsis. *Dev Cell* **43**, 630-642 e634,
848 doi:10.1016/j.devcel.2017.09.025 (2017).
849 48 Sorensson, C. *et al.* Determination of primary sequence specificity of Arabidopsis
850 MAPKs MPK3 and MPK6 leads to identification of new substrates. *Biochem J* **446**,
851 271-278, doi:10.1042/BJ20111809 (2012).
852 49 O'Donoghue, L. & Smolenski, A. Analysis of protein phosphorylation using Phos-tag
853 gels. *J Proteomics* **259**, 104558, doi:10.1016/j.jprot.2022.104558 (2022).
854 50 Mahfouz, M. M. *et al.* Targeted transcriptional repression using a chimeric TALE-
855 SRDX repressor protein. *Plant Mol. Biol* **78**, 311-321, doi:10.1007/s11103-011-9866-
856 x (2012).
857 51 Ueda, M. *et al.* Transcriptional integration of paternal and maternal factors in the
858 Arabidopsis zygote. *Genes Dev* **31**, 617-627, doi:10.1101/gad.292409.116 (2017).
859 52 Ueda, M., Zhang, Z. & Laux, T. Transcriptional activation of Arabidopsis axis
860 patterning genes WOX8/9 links zygote polarity to embryo development. *Dev Cell* **20**,
861 264-270, doi:10.1016/j.devcel.2011.01.009 (2011).
862 53 Herrmann, A. & Torii, K. U. Shouting out loud: signaling modules in the regulation
863 of stomatal development. *Plant Physiol* **185**, 765-780, doi:10.1093/plphys/kiaa061
864 (2021).
865 54 MacAlister, C. A., Ohashi-Ito, K. & Bergmann, D. C. Transcription factor control of
866 asymmetric cell divisions that establish the stomatal lineage. *Nature* **445**, 537-540,
867 doi:10.1038/nature05491 (2007).

868 55 Lampard, G. R., Macalister, C. A. & Bergmann, D. C. Arabidopsis stomatal initiation
869 is controlled by MAPK-mediated regulation of the bHLH SPEECHLESS. *Science*
870 **322**, 1113-1116, doi:10.1126/science.1162263 (2008).
871 56 Chen, H. *et al.* Phosphorylation-Dependent Activation of the bHLH Transcription
872 Factor ICE1/SCRM Promotes Polarization of the Arabidopsis Zygote. *New Phytol*,
873 2024.2007.2003.601926, doi:https://doi.org/10.1111/nph.20265 (2024).
874 57 Boutilier, K. *et al.* Ectopic expression of BABY BOOM triggers a conversion from
875 vegetative to embryonic growth. *Plant Cell* **14**, 1737-1749, doi:10.1105/tpc.001941
876 (2002).
877 58 De Rybel, B. *et al.* A bHLH complex controls embryonic vascular tissue
878 establishment and indeterminate growth in Arabidopsis. *Dev Cell* **24**, 426-437,
879 doi:10.1016/j.devcel.2012.12.013 (2013).
880 59 Mor, E. *et al.* bHLH heterodimer complex variations regulate cell proliferation
881 activity in the meristems of Arabidopsis thaliana. *iScience* **25**, 105364,
882 doi:10.1016/j.isci.2022.105364 (2022).
883 60 He, Q. *et al.* A receptor kinase complex refines cambium activity in Arabidopsis.
884 *bioRxiv*, 2024.2005.2016.594489, doi:10.1101/2024.05.16.594489 (2024).
885 61 Koch, G. W., Sillett, S. C., Jennings, G. M. & Davis, S. D. The limits to tree height.
886 *Nature* **428**, 851-854, doi:10.1038/nature02417 (2004).
887 62 *Harnessing Plants Initiative*, <https://www.salk.edu/harnessing-plants-initiative/>.
888 63 Lampropoulos, A. *et al.* GreenGate-a novel, versatile, and efficient cloning system for
889 plant transgenesis. *PLoS One* **8**, e83043, doi:10.1371/journal.pone.0083043 (2013).
890 64 Schurholz, A. K. *et al.* A Comprehensive Toolkit for Inducible, Cell Type-Specific
891 Gene Expression in Arabidopsis. *Plant Physiol* **178**, 40-53, doi:10.1104/pp.18.00463
892 (2018).
893 65 Ursache, R., Fujita, S., Denervaud Tendon, V. & Geldner, N. Combined fluorescent
894 seed selection and multiplex CRISPR/Cas9 assembly for fast generation of multiple
895 Arabidopsis mutants. *Plant Methods* **17**, 111, doi:10.1186/s13007-021-00811-9
896 (2021).
897 66 de Reuille, P. B. & Ragni, L. Vascular Morphodynamics During Secondary Growth.
898 *Methods Mol Biol* **1544**, 103-125, doi:10.1007/978-1-4939-6722-3_10 (2017).
899 67 Naseer, S. *et al.* Casparian strip diffusion barrier in Arabidopsis is made of a lignin
900 polymer without suberin. *Proc Natl Acad Sci U S A* **109**, 10101-10106,
901 doi:10.1073/pnas.1205726109 (2012).
902 68 Galaxy, C. The Galaxy platform for accessible, reproducible and collaborative
903 biomedical analyses: 2022 update. *Nucleic Acids Res* **50**, W345-W351,
904 doi:10.1093/nar/gkac247 (2022).
905 69 Schindelin, J. *et al.* Fiji: an open-source platform for biological-image analysis. *Nat*
906 *Methods* **9**, 676-682, doi:10.1038/nmeth.2019 (2012).

907

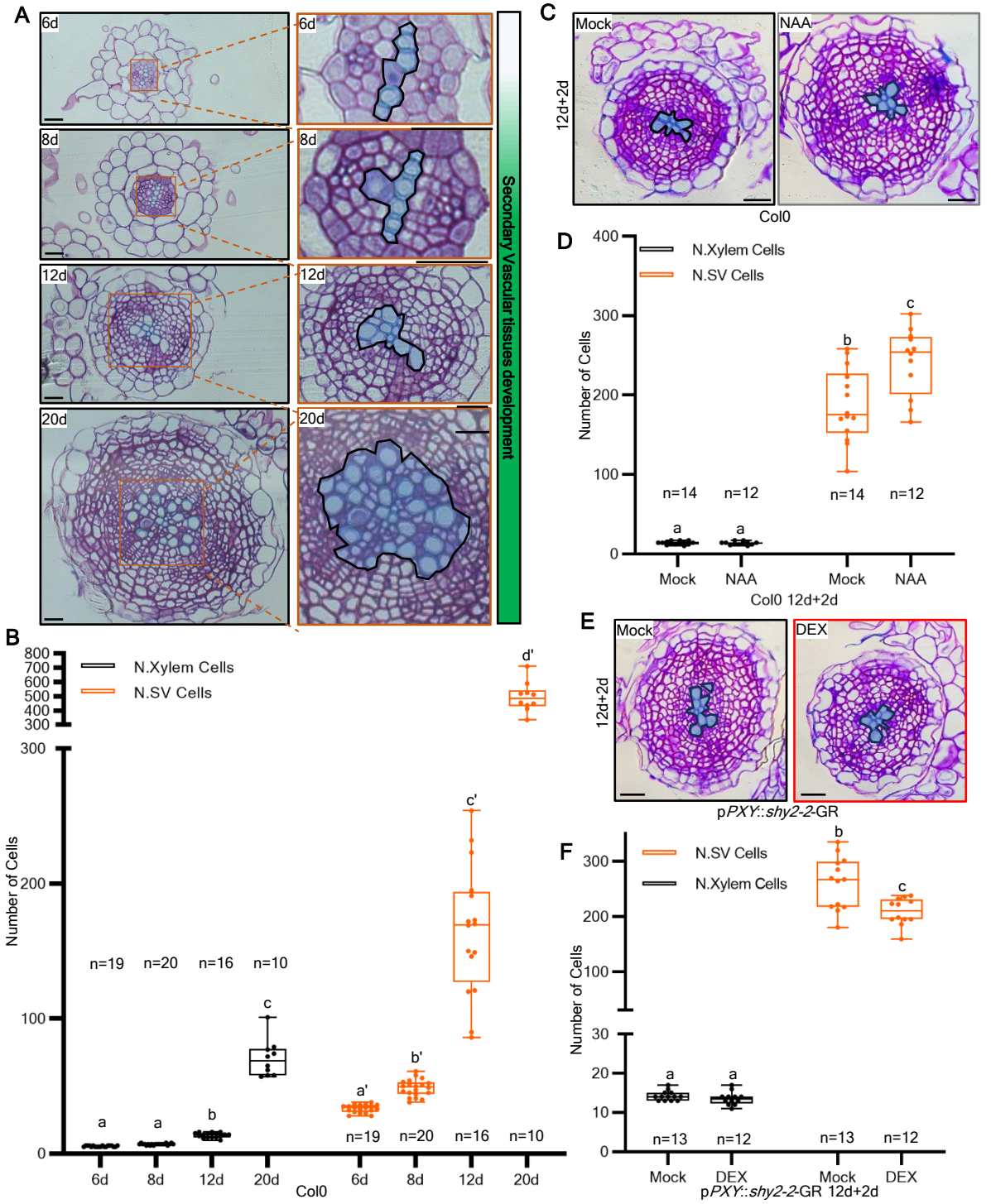

Fig. 1. Auxin signalling preferential controls the specific output of vascular cambium. (A), Secondary growth progression in the Arabidopsis root. Cross-sections of the most mature part of 6-day, 8-day, 12-day, and 20-day roots (*in vitro*). In the left panels, the orange squares indicate the magnification area shown in the right panels. Xylem cells are highlighted in blue. **(B)**, Quantification of secondary vascular (SV) tissue and xylem cell numbers of the experiment shown in (Fig1A). **(C)**, Cross-sections (plastic embedding) of the uppermost part of Col0 roots. 12-day-old plants were transferred to either Mock (left panel) or 1µM NAA (right panel) plates for 2 days. **(D)**, Quantification of the number of secondary vascular tissues and xylem cells in (Fig1C). **(E)**, Cross-sections (plastic embedding) quantification of the uppermost part of p*PXY*::*shy2-2*-GR roots (p*MYB84*::NLS-3xGFP and W131Y background); 12-day-old plants were transferred to either Mock (left panel) or 10 µM DEX (right panel) plates for 2 days. **(F)**, Quantification of the number of secondary vascular tissues and xylem cells in (Fig1E). The xylem vessels are highlighted in blue. Black scale bars: 20µm. Count data was modelled with a generalized mixed model. Here the Poisson mix model or Poisson model was selected. P-values were adjusted using Holm-Bonferroni correction.

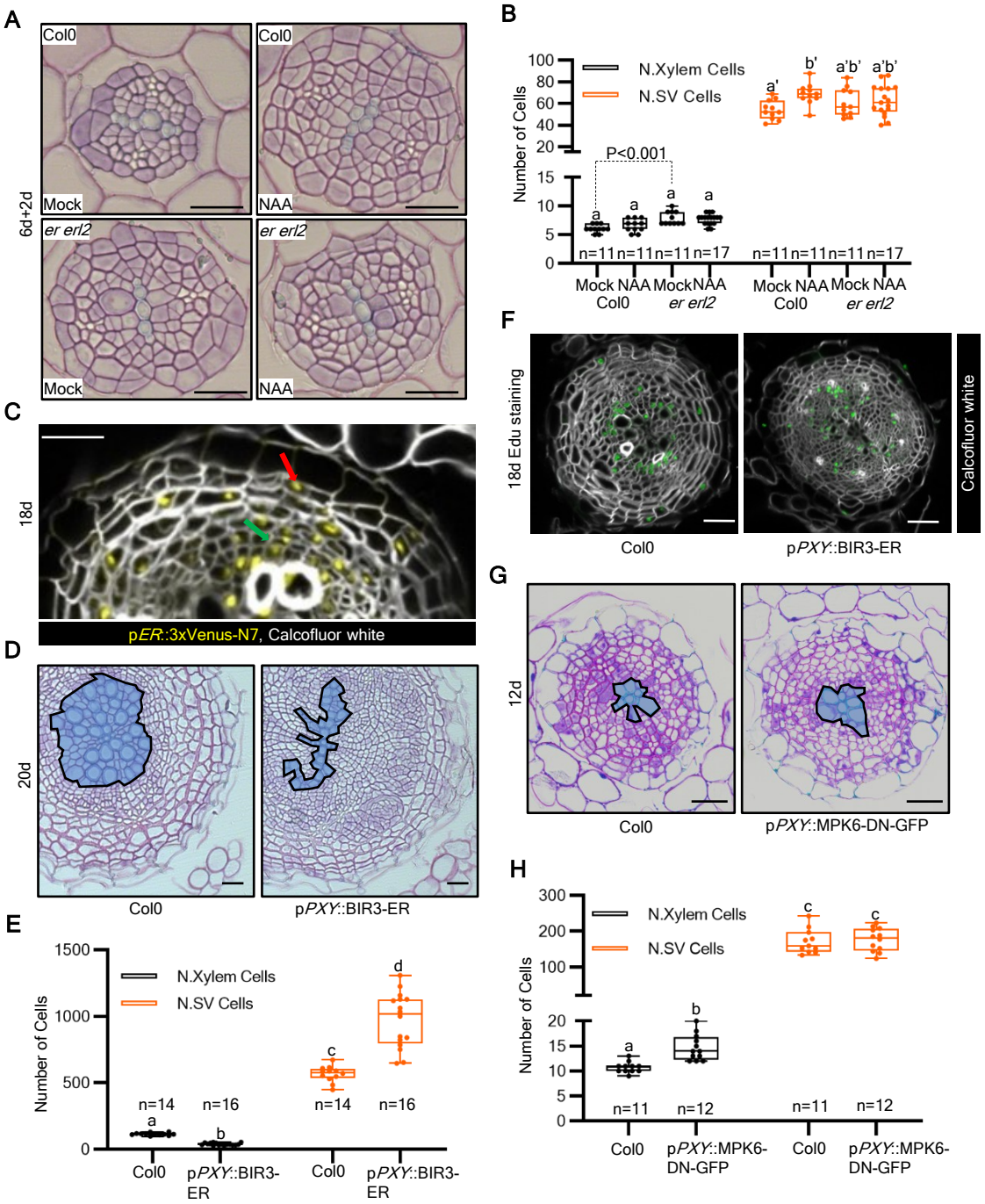

Fig. 2. The ERECTA and MPK6 kinase trigger the directional vascular cambium activity. (A), Cross-sections (plastic embedding) of the uppermost part of Col0 and *er erl2* roots. 6-day-old plants were transferred for 2 days on Mock (left panels) or 1µM NAA (right panels) plates. **(B)**, Quantification of the number of secondary vascular (SV) tissues and xylem cells in (Fig2A). **(C)**, Vibratome-sections of the uppermost part of 18-day-old p*ER*::3xVenus-N7 root. The red arrow indicates the cork cambium and the green arrow indicates the vascular cambium. **(D)**, Cross-sections (plastic embedding) of the uppermost part of 20-day-old Col0 (left panel) and p*PXY*::BIR3-ER (right panel) roots. The xylem vessels are highlighted in blue. **(E)**, Quantification of the number of secondary vascular tissues and xylem cells in (Fig2D). **(F)**, Edu staining of vibratome-sections of the uppermost part of 20-day-old Col0 (left panel) and p*PXY*::BIR3-ER (right panel) roots. **(G)**, Cross-sections (plastic embedding) of the uppermost part of 20-day-old Col0 (up-left panel) and p*PXY*::MPK6-DN-GFP (up-right panel) roots. The xylem vessels are highlighted in blue. **(H)**, Quantification of the number of secondary vascular tissues and xylem cells in (Fig2G). Black and white scale bars: 20µm. Count data was modelled with a generalized mixed model. Here the Poisson mix model was selected. P values were adjusted using Holm-Bonferroni correction. Count data was also analysed using the Student's T-test.

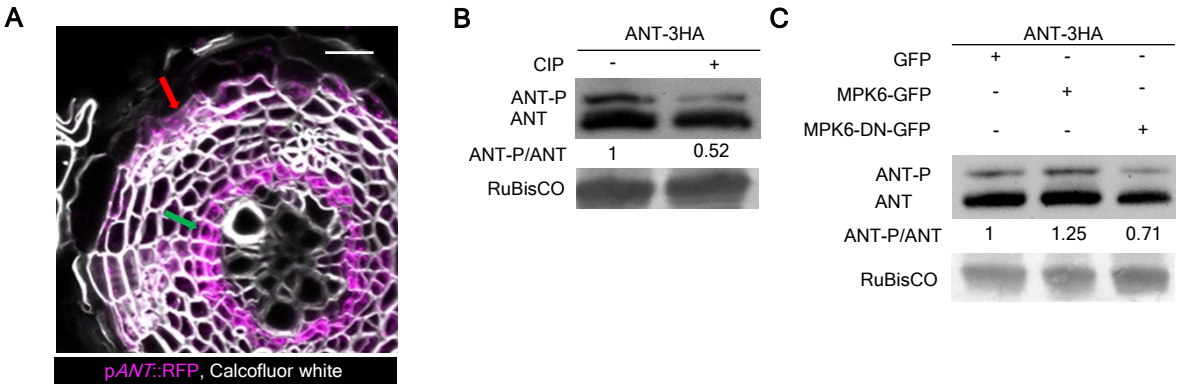

Fig. 3. ER phosphorylates ANT via the MPK6 kinase. (A), Vibratome-sections of the uppermost part of 18-day-old p*ANT*::RFP roots. The red arrow indicates the cork cambium and the green arrow indicates the vascular cambium. **(B)**, *In vivo* phosphorylation assays in *N. benthamiana*. Protein extracts, with or without treatment with Calf-intestinal alkaline (CIP), were analysed on a Phos-tag SDS-PAGE gel and probed with an anti-HA antibody. **(C)**, *In vivo* phosphorylation assays in *N. benthamiana*. p*35S*::ANT-3xHA were transiently expressed in leaves together with either p*35S*::MPK6-GFP or p*35S*::MPK6-DN-GFP (its dominant negative version). Protein extracts were analysed on a Phos-tag SDS-PAGE gel and probed with an anti-HA antibody. The relative concentration of phosphorylated ANT protein and unphosphorylated ANT protein was calculated using Fiji. White scale bars: 20µm.

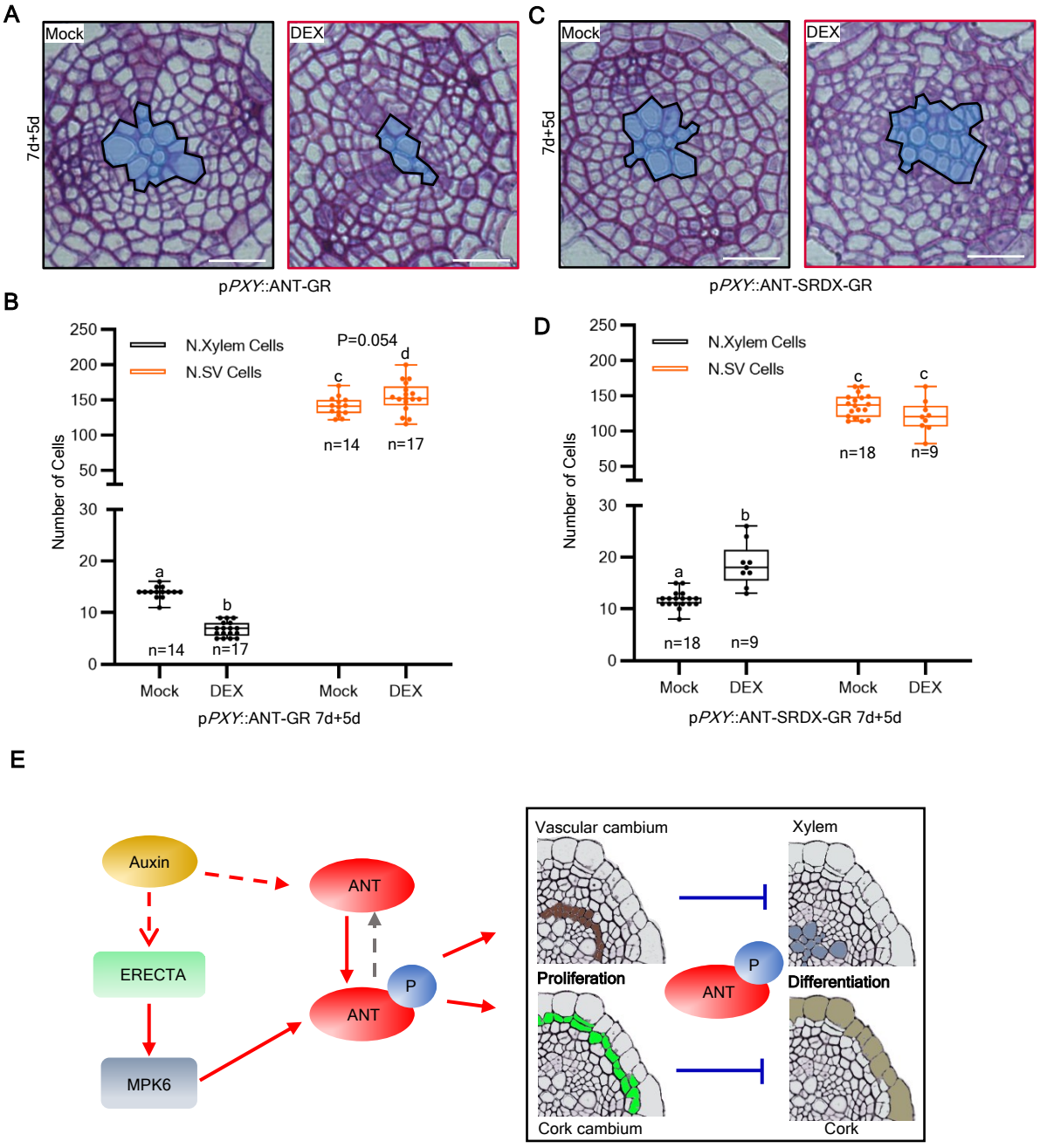

Fig. 4. ANT determines vascular cambium activity by repressing xylem cell formation. (A), Cross-sections (plastic embedding) of the uppermost part of 12-day-old p*PXY*::ANT-GR roots; 7-day-old plants were transferred to either Mock (left panel) or 10 µM DEX (right panel) plates for 5 days. **(B)**, Quantification of the number of secondary vascular (SV) tissues and xylem cells shown in (Fig4A). **(C)**, Cross-sections (plastic embedding) of the uppermost part of 12-day-old p*PXY*::ANT-SRDX-GR roots; 7-day-old plants were transferred to either Mock (left panel) or 10 µM DEX (right panel) plates for 5 days. **(D)**, Quantification of the number of secondary vascular tissues and xylem cells shown in (Fig4C). **(E)**, Model explaining cambia output specificity. The xylem vessels are highlighted in blue. White scale bars: 20µm. Count data was modelled with a generalized mixed model. Here the Poisson mix model was selected. P values were adjusted using Holm-Bonferroni correction. Count data was also analysed using the Student's T-test.